ACS OMEGA

Article

Cite This: ACS Omega 2019, 4, 10078−10088

http://pubs.acs.org/journal/acsodf

Poly(ethylene glycol)-Based Peptidomimetic "PEGtide" of Oligo-Arginine Allows for Efficient siRNA Transfection and Gene Inhibition

Alan Hibbitts,[†,∥,#,◆] Aoife M. O'Connor,[‡,◆] Joanna McCarthy,[▽] Éanna B. Forde,[‡] Gary Hessman,[⊥] Caitriona M. O'Driscoll,[▽] Sally-Ann Cryan,[†,§,∥,#,○] and Marc Devocelle*[,‡]

[†]Tissue Engineering Research Group, Department of Anatomy, [‡]Department of Chemistry, and [§]Drug Delivery & Advanced Materials Team, School of Pharmacy, Royal College of Surgeons in Ireland (RCSI), 123 St. Stephen's Green, Dublin 2, Ireland

[∥]Trinity Centre for Biomedical Engineering and [⊥]School of Chemistry, Trinity College Dublin (TCD), The University of Dublin, College Green, Dublin 2, Ireland

[#]Advanced Materials and Bioengineering Research (AMBER) Centre, RCSI & TCD, Dublin 2, Ireland

[▽]Pharmacodelivery Group, School of Pharmacy, University College Cork, Cavanagh Pharmacy Building, College Road, Cork T12 YN60, Ireland

[○]Centre for Research in Medical Devices (CURAM), NUIG & RCSI, Biomedical Sciences, National University of Ireland Galway (NUIG), Newcastle Road, Galway H91 W2TY, Ireland

Supporting Information

ABSTRACT: While a wide range of experimental and commercial transfection reagents are currently available, persistent problems remain regarding their suitability for continued development. These include the transfection efficiency for difficult-to-transfect cell types and the risks of decreased cell viability that may arise from any transfection that does occur. Therefore, research is now turning toward alternative molecules that improve the toxicity profile of the gene delivery vector (GDV), while maintaining the transfection efficiency. Among them, cell-penetrating peptides, such as octa-arginine, have shown significant potential as GDVs. Their pharmacokinetic and pharmacodynamic properties can be enhanced through peptidomimetic conversion, whereby a peptide is modified into a synthetic analogue that mimics its structure and/or function, but whose backbone is not solely based on α-amino acids. Using this technology, novel peptidomimetics were developed by co- and postpolymerization functionalization of substituted ethylene oxides, producing poly(ethylene glycol) (PEG)-based peptidomimetics termed "PEGtides". Specifically, a PEGtide of the poly(α-amino acid) oligo-arginine [poly(glycidylguanidine)] was assessed for its ability to complex and deliver a small interfering ribonucleic acid (siRNA) using a range of cell assays and high-content analysis. PEGtide−siRNA demonstrated significantly increased internalization and gene inhibition over 24 h in Calu-3 pulmonary epithelial cells compared to commercial controls and octa-arginine-treated samples, with no evidence of toxicity. Furthermore, PEGtide−siRNA nanocomplexes can provide significant levels of gene inhibition in "difficult-to-transfect" mouse embryonic hypothalamic (mHypo N41) cells. Overall, the usefulness of this novel PEGtide for gene delivery was clearly demonstrated, establishing it as a promising candidate for continued translational research.

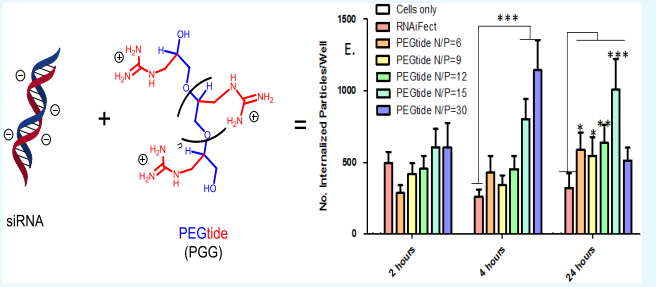

INTRODUCTION

Since its discovery, short interfering RNA (siRNA) has been under near-constant development as a potential therapy for a wide range of conditions.[1,2] Initially, research was focused on the more obvious targets of diseases with an underlying genetic cause such as cystic fibrosis[3,4] but has now expanded to more varied targets such as dry eye disease, hepatitis B, and solid tumors.[1] Following initial setbacks in the clinical translation of siRNA therapeutics, the technology is now experiencing a resurgence with the first Food and Drug Administration (FDA)-approved therapy, patisiran (Onpattro) by Alnylam, emerging for hereditary amyloidogenic transthyretin amyloidosis and several more now entering large-scale clinical trials.[1,5] However, a major issue remaining in developing siRNA therapeutic targets is the lack of suitable gene delivery vectors (GDVs) for most target organs. Poor cell uptake, toxicity, and immune cell activation are common issues reported among many synthetic vectors that otherwise display a promising level of gene inhibition.[2]

To avoid some issues observed concerning the administration of compounds that the body views as foreign, cell-penetrating peptides (CPPs) have been investigated as siRNA GDVs for a

Received: January 30, 2019
Accepted: May 29, 2019
Published: June 10, 2019

DOI: 10.1021/acsomega.9b00265
ACS Omega 2019, 4, 10078−10088

range of cell types/organs.[6] The oligo-arginine peptides, specifically octa-arginine (R8) and nona-arginine (R9) peptides, were identified as early candidates for the delivery of siRNA. From their preliminary studies, it was found that oligo-arginine–siRNA nanoparticles were capable of inducing gene knockdown to levels similar to or better than those observed with the reference CPP TAT.[7]

However, despite significant achievements in the field of peptide therapeutics, peptide-based candidates may have some shortcomings in clinical development.[8] To address some of these issues, efforts have led to the development of a class of molecules with peptide-like functions, known as "peptidomimetics". A peptidomimetic is a generic term describing a molecule that displays the biological activity of a parent peptide while being structurally different.[9−11] It can mimic a peptide primary structure through the use of amide bond isosteres and/or alteration of the native peptide backbone, including retro-inverso modification, chain extension, cyclization, or heteroatom incorporation.[11−13] This has been successfully applied to a range of clinical applications, including the development and optimization of antimicrobial peptides and cell-binding motifs.[10,14,15] Recently, work has also been undertaken to utilize the potential of the peptidomimetic technology in the delivery of biological macromolecules to generate targeted gene delivery vectors[16] or to improve the uptake ability and metabolic stability of preexisting CPPs.[17]

In addition to the peptidomimetic conversion, the modification of peptides and proteins with poly(ethylene glycol) (PEG) chains, termed pegylation, is another archetypal technique of structural adaptation for polyamide-based therapeutics.[21] However, the combination of these two approaches has not been attempted to date. Therefore, the synthesis of a novel PEG-based oligo-arginine peptidomimetic and evaluation of its capacity to complex and deliver siRNA are reported therein. This peptidomimetic would combine the previously described ability of polyarginines to effectively deliver siRNA with the improved safety profiles that have long been associated with PEGylation.[18,19] Specifically, PEG chains functionalized with groups resembling amino acid side chains and separated by an equal number of bonds compared to that in a peptide (Figure 1) were formed by a co- and postpolymerization functionalization approach. These hybrid structures of PEG and peptides, termed "PEGtides", are therefore different from the PEGtide dendrons that alternate monodisperse non-functionalized PEG chains and dipeptide Lys-β-Ala motifs.[20]

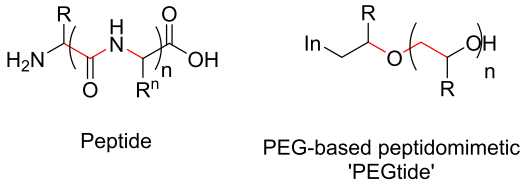

Figure 1. General structures of peptides and side-chain-functionalized poly(ethylene glycol)s as PEG-based peptidomimetics (R″: variable side chain; In: initiator).

Accordingly, a substituted oxirane was polymerized to form a functionalized PEG, which was modified to produce the oligo-arginine mimetic poly(glycidylguanidine) (PGG, **4**; Scheme 1). This CPP PEGtide, named thereafter PEGtide, was then tested for its ability to form nanocomplexes with siRNA, as well as to promote uptake and gene inhibition versus commercial controls. Its safety profile was also established. This allowed for the rapid evaluation of this novel molecule's future potential as a successful siRNA delivery vector.

RESULTS

PEGtide Synthesis. The poly(glycidylguanidine) (**4**) was produced in four synthetic steps in 16% overall yield (Scheme 1). Reactions were monitored by ^{1}H NMR and shown to be quantitative. The purification of the last intermediate was performed by size exclusion chromatography (SEC), and the final product (PEGtide) was analyzed by ^{1}H NMR and matrix-assisted laser desorption ionization time-of-flight mass spectrometry (MALDI-TOF MS).

The PEG backbone of this peptidomimetic was produced by anionic ring-opening polymerization of *tert*-butyl *N*-(2-oxiranylmethyl)carbamate, using potassium hydroxide as the initiator. Polymerization in the bulk monomer at 150 °C resulted in its complete conversion as well as the formation of *tert*-butylated amine repeating units by thermal decomposition of the *t*-Butyloxycarbonyl (Boc) group.[21] The latter was then removed from the polymer by treatment with trifluoroacetic acid. The deprotected primary amines were, in turn, reacted with *N*,*N*′-di-Boc-1*H*-pyrazole-1-carboxamidine, resulting in the guanylation of most repeating units. After SEC purification of this ultimate intermediate, the final deprotection of the guanidine groups was performed by treatment with trifluoroacetic acid, yielding poly(glycidylguanidine) (PGG). MALDI-TOF MS analysis was performed to characterize this product. The spectrum displayed main and fragmentation peak series, separated by 16 mass units, characteristic of PEG,[22,23] with molecular weight distributions based on a glycidylguanidine repeating unit. It also showed the presence of *tert*-butylated amine and free amine repeating units and a degree of polymerization for PGG ranging from 3 to 13 (Figure 2).

Accordingly, most PEGtide chains formed by this approach display the minimum net cationic charge required for the biological activity of the parent peptide. The polymerization of 1 g of monomer yielded 136 mg of PEGtide. The fractionation of this polymer into smaller ranges of repeating units was attempted by high-performance liquid chromatography (HPLC) (ion exchange chromatography, reversed phase (RP), SEC) but remained impracticable, so the polydisperse PEGtide (**4**) was tested for the transmembrane delivery of siRNA.

Size and ζ Potential of PEGtide–siRNA Nanoparticles. Following complex formation by electrostatic interaction, the physicochemical characteristics of the PEGtide–siRNA nanoparticles were assessed over a range of N/P ratios (Figure 3). It was found that large nanoparticles of size approximately 540–580 nm were observed at lower N/P ratios. The PEGtide–siRNA nanoparticle size decreased to 298 nm at the highest value of N/P = 30. Similarly, the polydispersity indices (PDIs) also demonstrated increasing homogeneity, with increasing N/P ratios, with N/P = 15 and 30 both giving the lowest PDIs of 0.2. The analysis of the surface charge revealed that PEGtide–siRNA complexes formed increasingly cationic nanoparticles with increasing N/P ratios. However, most of the nanoparticles retained an overall anionic charge with fully cationic particles only forming at N/P = 30.

Multiparameter Analysis of PEGtide–siRNA Nanoparticle Toxicity in Calu-3 Cells. High-throughput multiparameter methods were harnessed to rapidly screen for the toxicity of PEGtide–siRNA nanoparticles in Calu-3 cells. The nanoparticles were assessed using Calu-3 cells that were

DOI: 10.1021/acsomega.9b00265
ACS Omega 2019, 4, 10078−10088

Scheme 1. Synthetic Route to Poly(glycidylguanidine) (4), Starting from (±)-*tert*-Butyl *N*-(2-Oxiranylmethyl)carbamate

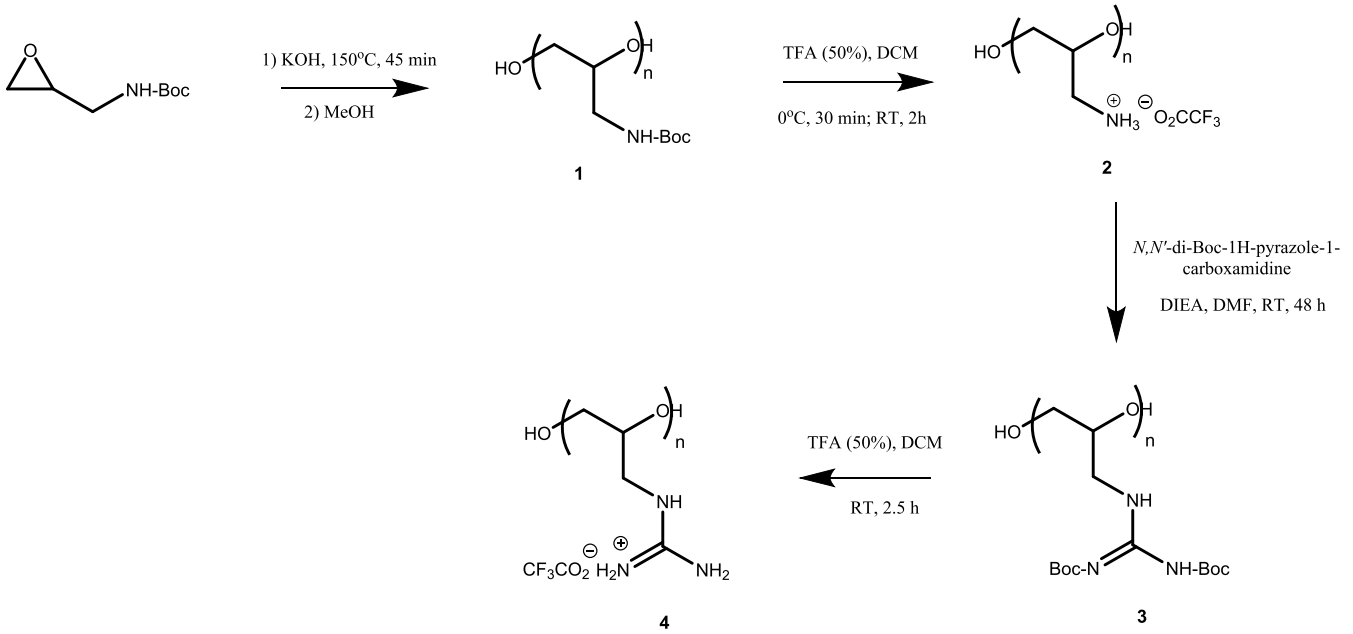

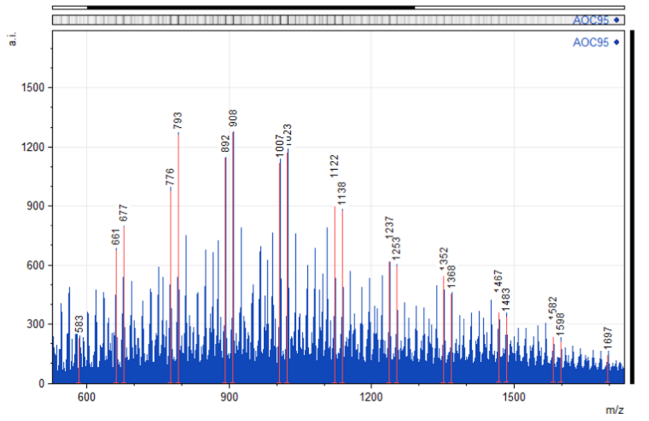

Figure 2. MALDI-TOF MS spectrum of poly(glycidylguanidine). The molecular weight distributions of 677, 793, 908, 1023, 1138, 1253, 1368, 1483, and 1598 are from the main series, and the molecular weight distributions of 661, 776, 892, 1007, 1122, 1237, 1352, 1467, 1582, and 1697 are from the fragmentation peak series. A version of this spectrum labeled with exact masses is available in the Supporting Information.

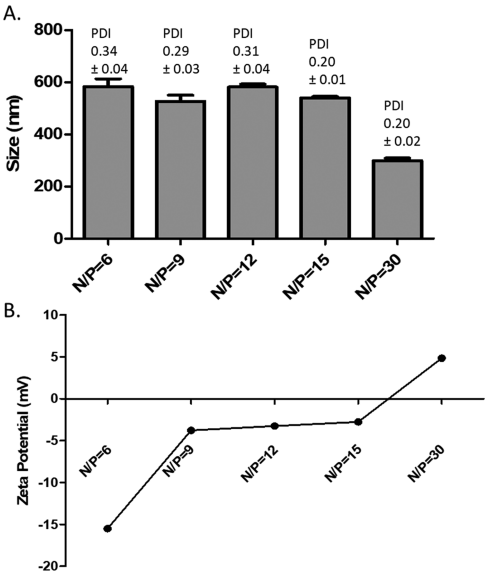

Figure 3. (A) Particle size and polydispersity indices and (B) ζ potential of PEGtide−siRNA nanoparticles at N/P ratios of 10−100 [±standard error of the mean (SEM), $n = 5$].

incubated with 100 nM siRNA per well over a range of peptidomimetic/siRNA ratios for 24 h. Thereafter, cell viability and nanoparticle-mediated toxicity were qualitatively and quantitatively determined using the Cellomics Multiparameter Cytotoxicity 3 kit and InCell 1000 Workstation software for analysis.

The analysis of the data revealed that PEGtide−siRNA nanoparticles remained well tolerated at all doses subsequently shown to facilitate siRNA uptake, with significant decreases in the cell number only observed at the higher N/P ratios of N/P = 60 and 100 (Figure 4A). However, these were only examined to illustrate a dose response at very high doses.

The analysis of the cell death-associated characteristics was also carried out. The examination of the changes observed in the mitochondrial membrane potential (MMP) following nanoparticle administration yielded conflicting results (Figure 4B). Some small MMP decreases in PEGtide−siRNA nanoparticle-treated cells were observed at N/P = 12 and 60; however, there appeared to be no correlation with the dose, thereby resulting in no definite conclusions being drawn from this parameter. The analysis of cytochrome *c* release from PEGtide−siRNA-treated cells demonstrated no significant changes, regardless of the N/P ratios applied, while a significant increase observed with the positive control valinomycin confirmed that the assay functioned as expected (Figure 4C). The examination of the changes elicited in the plasma membrane permeability (PMP) levels, however, resulted in much clearer indications of cytotoxicity at higher doses (Figure 4D). Overall, the use of PEGtide−siRNA nanoparticles was well tolerated and resulted in no significant changes in PMP except at the higher N/P ratios of 60 and 100.

DOI: 10.1021/acsomega.9b00265
ACS Omega 2019, 4, 10078−10088

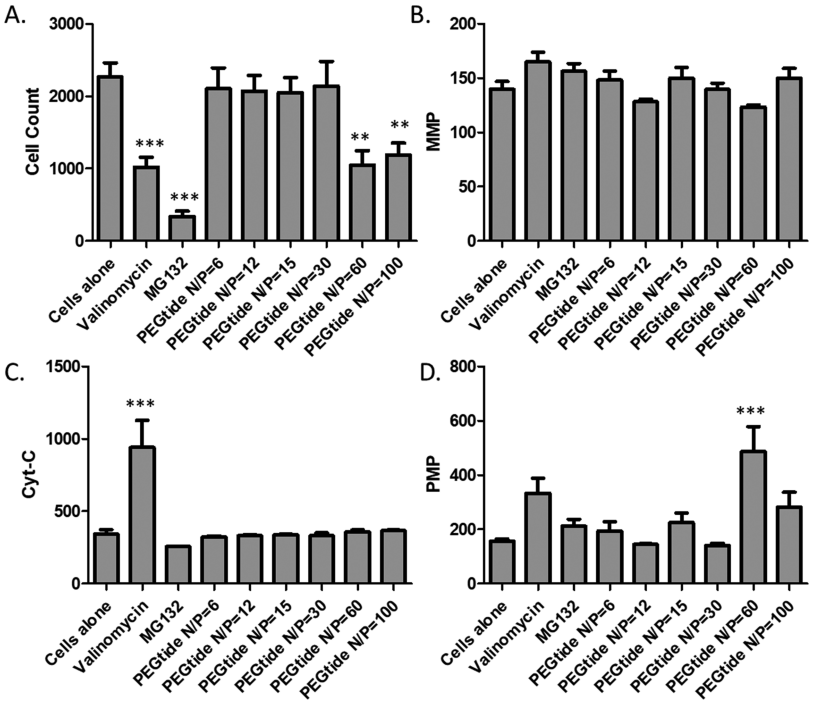

Figure 4. Quantitative high-content analysis (HCA) of valinomycin and MG132 positive controls and PEGtide−siRNA-nanoparticle-mediated toxicity in Calu-3 cells measured at 24 h post-administration. (A) Cell count, (B) mitochondrial membrane potential (MMP), (C) cytochrome *c* (Cyt *c*) release, and (D) plasma membrane permeability (PMP). *Y* axes represent the fluorescence intensity in arbitrary units (a.u.) (one-way analysis of variance vs untreated cells, $n = 3 \pm$ SEM, * $p < 0.05$, ** $p < 0.01$, *** $p < 0.001$).

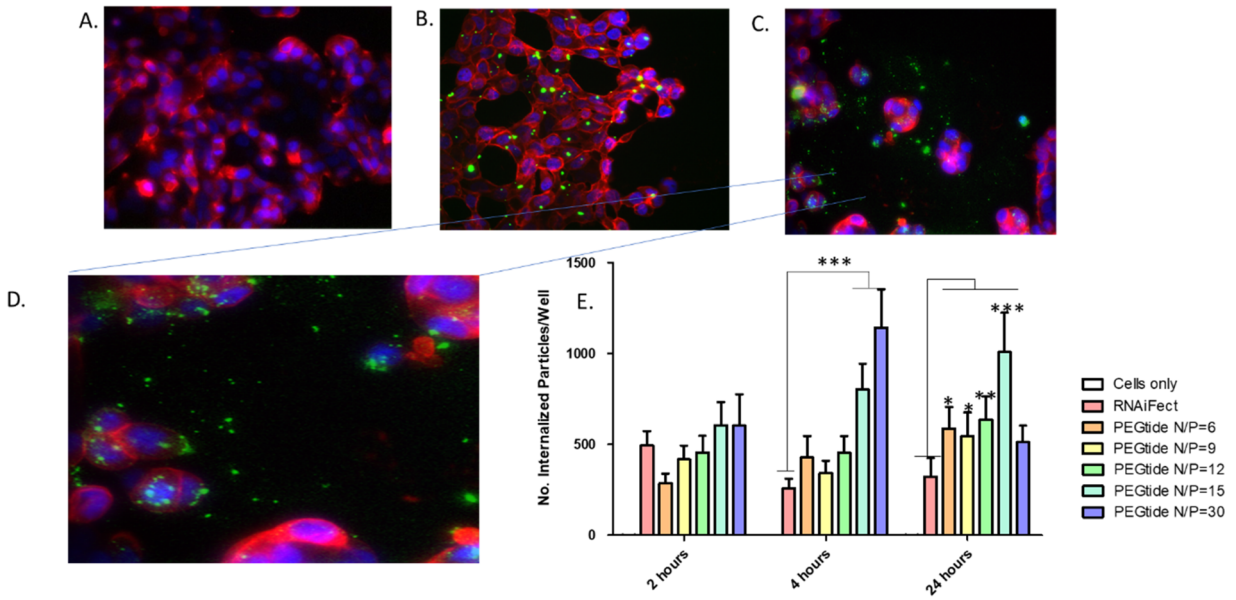

Figure 5. HCA 20× fused image analysis of PEGtide−siRNA uptake in Calu-3 cells 24 h post-transfection. The cells were treated with 100 nM of FITC-tagged siRNA nanoparticles (green) and were subsequently stained for cell nuclei using Hoechst nuclear stain (blue) and cell membrane using phalloidin−tetramethylrhodamine B isothiocyanate (TRITC) (red). (A) Untreated cells, (B) RNAiFect, (C) PEGtide N/P = 9, (D) expanded view of PEGtide N/P = 15, and (E) quantitative HCA analysis of RNAiFect vs PEGtide−siRNA nanoparticle uptake in Calu-3 cells measured at 2, 4, and 24 h post-administration (two-way ANOVA, $n = 3 \pm$ SEM, * $p < 0.05$, ** $p < 0.01$, *** $p < 0.001$).

Analysis of PEGtide−siRNA Nanoparticle Uptake in Calu-3 Cells. The ability of the PEGtide−siRNA nanoparticles to facilitate siRNA uptake by Calu-3 cells was assessed using high-content analysis (HCA) and was compared to a benchmark, lipid-based, transfection reagent (RNAiFect). Calu-3 cells were treated with fluorescein isothiocyanate (FITC)-tagged siRNA−PEGtide nanoparticles using mimetic/siRNA ratios ranging from 6 to 30. Thereafter, the cells were incubated for 2, 4, or 24 h prior to HCA quantification (Figure 5). At 2 h post-treatment, there was no significant difference in nanoparticle uptake between PEGtide−siRNA nanoparticles and RNAiFect−siRNA nanoparticles. However, when the incubation time was increased to 4 h, there were significantly higher levels of nanoparticle uptake in the PEGtide−siRNA nanoparticles at N/

DOI: 10.1021/acsomega.9b00265
ACS Omega 2019, 4, 10078−10088

P = 15 and 30. The levels of PEGtide−siRNA nanoparticle uptake continued to increase at 24 h post-treatment and led to significantly higher levels of siRNA internalization than in RNAiFect−siRNA-treated cells, at all N/P ratios, except 30, where no significant difference between the two nanoparticles was observed.

PEGtide−siRNA Nanoparticle Knockdown. To examine the ability of PEGtide−siRNA nanoparticles to effect gene knockdown, luciferase-expressing Calu-3 cells were transfected with 100 nM antiluciferase siRNA for 24 h using optimal conditions (Figure S8), and the results were analyzed (Figure 6A). At lower N/P ratios, there was no significant difference between the peptidomimetic nanoparticles and RNAiFect-treated samples. However, at N/P = 15 and 30, the knockdown efficiency of peptidomimetic nanoparticles was significantly higher than commercial controls with levels of knockdown as high as 68.56 ± 12.85%. In contrast to its peptidomimetic, it was found that octa-arginine transfection did not demonstrate significant improvement in gene knockdown compared to RNAiFect. Indeed, PEGtide−siRNA-mediated luciferase knockdown was significantly higher than octa-arginine-transfected samples at N/P = 30.

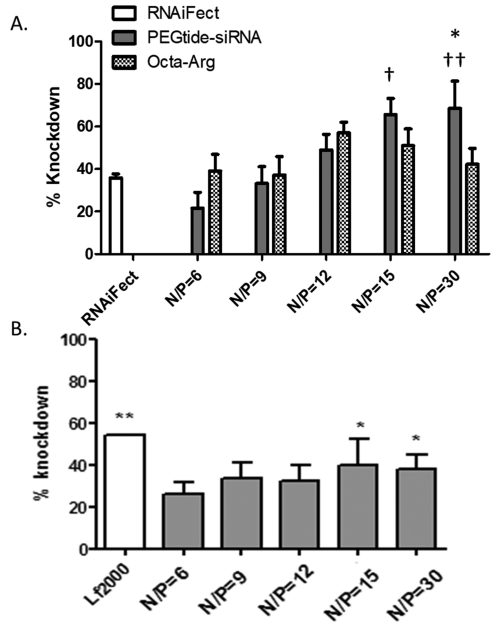

Figure 6. (A) Percentage of luciferase knockdown in Calu-3 cells after treatment with PEGtide−siRNA or octa-arginine siRNA nanoparticles vs nontargeting controls using 100 nM of antiluciferase siRNA 24 h post-transfection (two-way ANOVA, $n = 3 \pm$ SEM, † $p < 0.05$ †† $p < 0.01$, † vs RNAiFect, * vs octa-arginine). (B) Percentage of luciferase knockdown in difficult-to-transfect N41 neuronal cells demonstrated significant levels of knockdown that were comparable to those in commercial controls (one-way ANOVA, $n = 3 \pm$ SEM, * $p < 0.05$, ** $p < 0.01$, significance vs nontargeting controls).

Finally, PEGtide−siRNA particles were also examined in the N41 neuronal cell line to demonstrate the efficacy in a known cell type that is commonly seen as difficult to transfect (Figure 6B). Using this cell line, it was observed that PEGtide−siRNA was capable of significant levels of gene inhibition at N/P = 15 and 30 against negative controls. Furthermore, the levels of gene knockdown were also comparable to those of the Lipofectamine positive controls.

DISCUSSION

No standard method has been reported to convert a peptide into a peptidomimetic. The structural modification can be from conservative to extreme, but peptidomimetic transformations tend to focus on the linear (polyamide) backbone of the peptide. The latter is the target of degradative enzymes; consequently, peptidomimetic conversions generally aim to replace the polyamide chain by an analogous non-natural backbone. Many peptidomimetic structures and approaches have been developed.[24] However, these methods generally use synthetic approaches reminiscent of peptide synthesis, following a stepwise approach, where each amino acid derivative or analogue is sequentially added to a growing chain. Therefore, we have chosen an alternative strategy, based on a recently introduced polymerization technique, which generates a linear backbone analogous to the peptide's polyamide chain. However, polymer-based peptidomimetics of the oligo-arginine CPP were successfully developed such as guanidinylated poly((oxa)-norbornenes), polymethacrylamides, and oligo- and polycarbonates, as well as guanidinylated polymethacrylates,[25−27] and this technique has not yet been applied to PEG. Considering that it was described as "the gold standard biocompatible polymer for pharmaceutical and medical applications",[11] PEG represents a highly attractive moiety to replace the polyamide backbone of a peptide. The polymerization of functionalized ethylene oxides and their subsequent modification can yield PEG-based peptidomimetics of sequence-independent peptides. We applied this peptidomimetic conversion here to a homopoly(α-amino acid) representative of a class of peptidic delivery agents to create a hybrid structure of PEG and a peptide that we have termed a "PEGtide". Consistent with the polymerization technique used, the material obtained is a polydisperse polymer. However, anionic ring-opening polymerization, such as the one used here, is likely to provide better control over the molecular weight distribution than cationic ring-opening polymerization.[14] It is noteworthy that the PEG-based peptidomimetic PEGtide was produced from a racemic substituted oxirane and is therefore optically inactive. This could impact the ability of the PEGtide to complex a homochiral cargo such as a siRNA. However, homochiral polymers themselves would be associated with higher production costs. It should also be considered that the biological activities of CPPs can be independent of the stereochemistry of their constitutive amino acids,[28] although heterochiral CPPs and racemic mixtures of these peptides are generally not used. Whether the use of monodisperse and/or homochiral PEGtides provide even higher transfection efficiencies will be investigated in the future. While it will most likely be necessary to further refine either the synthesis or purification for progression toward clinical applications, the use of polydisperse transfection reagents is more acceptable in an in vitro setting. Examples of these are widely used in the fields of gene delivery and biomaterials (e.g., polyethylenimine and chitosan).[29,30]

When the PEGtide was complexed to siRNA, it was found to form complexes in the nanorange with an increasing cationic surface charge corresponding to an increasing N/P ratio, with a fully cationic surface charge not observed until N/P > 15. This is most likely because the full condensation of the siRNA is only achieved at this point. This is consistent with the previously described relationship between siRNA condensation and increasing N/P ratio.[31,32]

DOI: 10.1021/acsomega.9b00265
ACS Omega 2019, 4, 10078−10088

Overall, size distribution was similar to current CPP-based transfection platforms (e.g., the PepFect system)[33,34] and other peptidomimetic constructs.[35] Considering the large size of these particles relative to other nanoparticles, it is most likely a result of the use of phosphate-buffered saline (PBS) as a dispersant in complexation. This is indeed known to exert a significant influence on the size and surface charge of siRNA nanocomplexes.[36,37] Furthermore, the lower charge density and PEG backbone of the PEGtide itself are also known to exert an effect on nanoparticle size and charge. Recent studies involving a range of PEGylated polymers have highlighted the effect that PEG molecular weights and grafting densities can have on particle size and ζ potential.[38] Specifically, Moore et al. also demonstrated that varying the level of cationic grafting to a PEG backbone can result in nucleic acid nanoparticle sizes ranging from 200 to 500 nm.[39] Furthermore, decreases in ζ potentials following PEGylation of CPPs have also been reported.[40] Finally, there are numerous reports indicating that incubation in serum will have dramatic effects on particle size and charge. Specifically, work by Kummitha et al.[41] and Strojan et al.[42] using a range of particle types found that size and polydispersity dramatically increase following exposure to serum. However, considering the high levels of gene inhibition observed in this study, serum-PEGtide interactions did not pose an insurmountable obstacle to cell endocytosis.

Using a multiparameter HCA approach, PEGtide−siRNA nanoparticles were found to be well tolerated with no indications of toxicity up to N/P = 60 and 100 using 100 nM of siRNA. At these N/P ratios, the cell numbers were significantly reduced, and PMP was found to be significantly enhanced as was previously reported at cytotoxic levels using this approach.[36] While the cell numbers were found to be dose-dependent in a clear fashion, the additional cytotoxic parameters provided additional details on the nature of the cytotoxic mechanism in action. This was most evident in the staining for cytochrome *c* release. While treatment with both valinomycin and MG132 resulted in significant decreases in the cell number, only treatment with valinomycin resulted in significant release of cytochrome *c*. Although both positive controls are known to induce apoptosis via cytochrome *c* release and subsequent caspase cascade,[43] it is also possible that the more potent MG132 is also inducing cell death via caspase-independent cell death such as autophagy. This mode of cell death has been found to occur independently of caspase release,[44] although there is a large amount of cross-talk between the two mechanisms. The safety profile of these PEGtides was further clarified compared to previously established toxicities of commercial gene delivery vectors. Specifically, studies by Breunig et al. demonstrated that following lipofectamine use, at comparable nucleic acid concentrations to those used in this study, decreases in cell viability of 12−47% were observed.[45] Furthermore, toxicity profiles determined by the PEGtide approach described here represent an improvement on previous efforts by the authors with octa-argine grafting, which demonstrated decreases in viability of 15−40%.[46]

To analyze a large array of time points and doses, HCA methods were employed, similar to those previously described in industrial and research applications.[36] When assessed for uptake into Calu-3 cells, PEGtide−siRNA nanoparticles did not demonstrate any significant difference from RNAiFect until 4 h post-treatment. This lower rate of uptake for anionic particles would also be in keeping with the difficulties expected from anionic or weakly cationic particles interacting with the negatively charged cell membrane. The polydispersity of some of the lower N/P ratios results in some uncertainty regarding their behavior; most likely, there is a subpopulation of smaller particles that possess a size and charge amenable to endocytosis. While the ζ potential for these N/P ratios is negative, studies have found that negatively charged particles can internalize via clathrin-mediated endocytosis.[47]

Specifically, at 4 h post-treatment, the only PEGtide−siRNA nanoparticles that had significantly higher levels of siRNA uptake compared to RNAiFect−siRNA nanoparticles were the most compact and cationic ones (N/Ps = 15 and 30). However, when tested at 24 h post-treatment and N/P ratios ranging from 6 to 15, the levels of siRNA uptake were significantly higher with PEGtide than with RNAiFect. Considering the PEGtide−siRNA nanoparticle size and surface charge, it is likely that they are transient aggregations based on their microenvironment but that dispersion and subsequent transfection ultimately occur (albeit at a much reduced rate). This was found to be the case using other nanoparticle systems and has even been used as a strategy for targeting the lungs.[48,49]

Interestingly, a decrease in uptake levels was also observed from 4 to 24 h in PEGtide−siRNA samples at N/P = 30. Since these nanoparticles were observed to be internalized at the highest rate, this drop was likely a result of faster overall cycling through the cell trafficking machinery. The result is either exocytosis via egress of the PEGtide−siRNA from late endosomes/lysosomes (≅70% of the internalized siRNA)[50] or final degradation in the lysosome. This was previously found to be the case for 99% of delivered particles that are not ejected[51] and would explain the apparent drop in the number of internalized PEGtide−siRNA particles.

The PEGtide delivery of siRNA to Calu-3 cells resulted in the efficient knockdown of ∼70% at N/P = 30. These levels of knockdown were significantly higher than both RNAiFect commercial controls and luciferase knockdown obtained using the same N/P ratio of traditional octa-arginine. When comparing against the earlier uptake experiments, we note that while uptake was faster overall at N/P = 30, there was no significant difference between N/P = 15 and 30. This is reflected in the gene knockdown data described and we contend that this is most likely a result of all available RNA-induced silencing complex machinery becoming saturated or approaching a point of saturation at the 24 h mark.

Furthermore, PEGtide delivery of siRNA provided significant levels of gene knockdown in the "hard-to-transfect" N41 neuronal cell line at a level approaching those achieved with commercially available Lipofectamine 2000 (Lf2000). It is also worth considering that the PEGtide−siRNA system described here is relatively low in molecular weight, simple in structure, and can be formed in a four-step reaction procedure from relatively inexpensive reagents. This should allow for successful future scale-up and testing in more complex in vitro and in vivo models.

CONCLUSIONS

With siRNA now achieving FDA approval for certain indications, it remains imperative that there are appropriate carriers for safe and efficient delivery for a range of diseases and organs. The PEGtide system described in this paper has demonstrated a strong capability for nanoparticle formation combined with a low-toxicity profile and high levels of gene inhibition. It also represents a flexible system amenable to applications that may encompass those that have been

DOI: 10.1021/acsomega.9b00265
ACS Omega 2019, 4, 10078−10088

successfully implemented with CPPs, including the delivery of proteins, liposomes, nanoparticles, and larger nucleic acids, such as those used by the CRISPR/Cas-9 gene editing technology.

EXPERIMENTAL SECTION

Materials. The Fmoc-protected amino acids and Rink Amide 4-methylbenzhydrylamine (MBHA) resin for peptide synthesis were obtained from Novabiochem (Nottingham, U.K.). Hexafluorophosphate azabenzotriazole tetramethyl uronium (HATU) and *N*-methyl-2-pyrrolidone (NMP) were purchased from ChemPep Inc. (Wellington, FL) and Bio-Sciences (Dublin, Ireland), respectively. All other reagents and solvents were sourced from Sigma-Aldrich (Dublin, Ireland) except where indicated. siGENOME nontargeting siRNA #2 (5′ UAAGGCUAUGAAGAGAUAC 3′) was obtained from Dharmacon (Lafayette, CO). The nontargeting sequence #2 is nonspecific for human gene sequences and specific for firefly luciferase using the Promega pGL3 cloning vector. AllStars negative control siRNA was obtained from Qiagen (Manchester, U.K.). This siRNA has no homology to any known mammalian gene and has been validated using Affymetrix GeneChip arrays and a variety of cell-based assays. AllStars negative control siRNA was also obtained from Qiagen with a fluorescein isothiocyanate (FITC) modification for cell uptake studies.

General Experimental Methods. NMR spectra were recorded using a Bruker Avance 400 spectrometer. MALDI-TOF MS analysis was performed either on an AB Sciex 4800 MALDI-TOF/TOF (Cheshire, U.K.), using α-cyano-4-hydroxy-cinnamic acid as a matrix, or a Waters MALDI Q-Tof Premier Mass Spectrometer (Milford, MA), using *trans*-2-[3-(4-*tert*-butylphenyl)-2-methyl-2-propenylidene]malononitrile as a matrix.

Synthetic Procedures and Analytical Data. *Octa-D-Arginine Synthesis.*

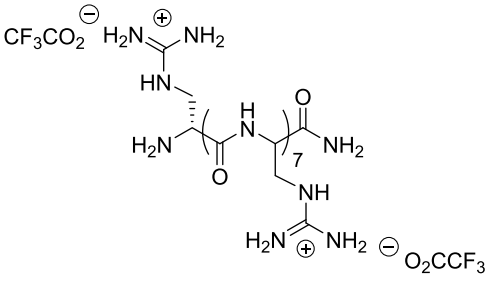

This peptide was assembled by standard solid-phase peptide synthesis[52] according to the Fmoc-*t*Bu strategy[53] with HATU/*N*,*N*-diisopropylethylamine (DIEA) coupling chemistry in NMP solvent. Single-coupling cycles, using a total 10-fold excess of Fmoc-D-Arg(Pbf)-OH to resin-bound peptide, were used. Assembly of the amino acid sequence, starting from a Rink Amide MBHA resin, was carried out on a 100 μmol scale using a 433 Applied Biosystems automated peptide synthesizer (Warrington, U.K.). The peptide was deprotected and released from the resin by treatment with a cleavage cocktail consisting of 95% trifluoroacetic acid, 2.5% water, and 2.5% triisopropylsilane for 4.5 h. The peptide was then precipitated from this solution with diethyl ether, isolated by centrifugation, and washed three times with diethyl ether. It was next air-dried, dissolved in distilled water, and lyophilized.

Chromatographic analysis and purification were performed by RP-HPLC using the Varian Galaxy HPLC (Walnut Creek, CA) and PerSeptive BioSystems BioCad Sprint Perfusion Chromatography HPLC (Warrington, U.K.), respectively, and Phenomenex Jupiter 5 μm C5 300 Å columns, 4.6 mm D × 250 mm L analytical; 10 mm D × 250 mm L semipreparative (Macclesfield, U.K.). The mobile phase consisted of buffer A: 0.1% trifluoroacetic acid (TFA) in water and buffer B: 0.1% TFA in acetonitrile, with a linear gradient of 5−65% B in 30 min at a flow rate of 1 mL/min (analysis) or 4 mL/min (semipreparative). UV single-wavelength detection was performed at 214 nm for the BioCad Sprint, while the Varian Galaxy was equipped with a photodiode array (PDA) detector operating from 190 to 950 nm. Purity was ascertained from the percent area of octa-arginine relative to the total area of all UV-absorbing components.

Analytical HPLC (C5): t_R = 11.53 min, 89% purity.

MALDI-TOF MS (m/z) (α-cyano-4-hydroxy-cinnamic acid) calcd for $C_{48}H_{100}N_{33}O_8$: 1266.843. Found: 1266.839.

Poly(glycidylguanidine) (PGG) Synthesis.

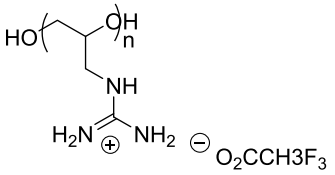

(n = 3-13)

*Poly(glycidyl tert-butylcarbamate) (**1**).* Polymerization was performed in the bulk monomer: *tert*-butyl *N*-(2-oxiranylmethyl)carbamate (1.02 g, 5.9 mmol) was introduced in a round-bottom flask maintained at 50 °C. Potassium hydroxide (16.5 mg, 0.29 mmol) was added under nitrogen, and the solution was stirred at 150 °C for 45 min. When the polymer had begun to solidify, the polymerization was quenched by adding methanol (2 mL), which was then removed under vacuum, providing poly(glycidyl *tert*-butylcarbamate) in quantitative yield.

^{1}H NMR (400 MHz, $CDCl_3$) δ = 3.84−2.98 (m, CH_2O, CH_2N and CH, 6H), 1.37 (s, CH_3 Boc, 9H), 1.20 (s, CH_3 *t*-Bu, 3H).

The signal at 1.20 ppm is attributed to *tert*-butylated amine repeating units (vide infra). Complete conversion of the monomer is shown by the absence of signals at 2.59 and 2.40 ppm (CH_2O).

*Poly(glycidylamine) (**2**).* Boc deprotection was carried out by dissolving poly(glycidyl *tert*-butylcarbamate) (1.02 g, 5.9 mmol) in a mixture of dichloromethane (3 mL) and trifluoroacetic acid (3 mL). This solution was stirred in an open flask at 0 °C for 30 min, followed by 2 h at room temperature (RT). The solvent was then removed by evaporation using a stream of nitrogen. The residue was dissolved in water, and the solution was freeze-dried. Poly(glycidylamine) was recovered as a yellow oil in quantitative yield.

^{1}H NMR (400 MHz, D_2O) δ = 3.86−2.93 (m, CH, CH_2O and CH_2N, 339 H), 1.08 (s, CH_3 *t*-Bu, 9H).

The signal at 1.08 ppm is attributed to *tert*-butylated amine repeating units. Successful deprotection was shown by the reduction near to the baseline of the signal at 1.40 ppm (CH_3 Boc).

*Poly(glycidyl N,N′-di-Boc-guanidine) (**3**).* To a solution of poly(glycidylamine) (500 mg, 6.85 mmol) in dimethylformamide (10 mL), *N*,*N*′-di-Boc-1*H*-pyrazole-1-carboxamidine (4.2 g, 13.7 mmol) and DIEA (4.76 mL, 27.4 mmol) were added. The resulting yellow solution was stirred at room temperature for 48 h. Water (50 mL) was then added, and the solution was extracted with chloroform. The organic phase was subjected to

DOI: 10.1021/acsomega.9b00265
ACS Omega 2019, 4, 10078−10088

size column chromatography (Sephadex LH 20 as the stationary phase and methanol as the mobile phase); 400 mg (18%) of product was recovered.

^{1}H NMR (400 MHz, $CDCl_3$) δ = 11.40 (bs, NH, 1H), 8.56 (bs, NH, 1H), 3.93−3.17 (m, CH, CH_2O and CH_2N, 8H), 1.40 (s, CH_3, 18H).

*Poly(glycidylguanidine) (PGG, **4**).* Boc deprotection was carried out by dissolving polyglycidyl *N,N′*-di-Boc-guanidine (400 mg, 1.23 mmol) in a mixture of dichloromethane (3 mL) and trifluoroacetic acid (3 mL). This solution was stirred in an open flask at 0 °C for 30 min, followed by 2 h at room temperature. The solvent was then removed by evaporation using a stream of nitrogen. The residue was dissolved in water, and the solution was freeze-dried. Poly(glycidylguanidine) was recovered as a yellow oil (136 mg, 95%).

^{1}H NMR (400 MHz, D_2O) δ = 3.90−2.96 (m, CH, CH_2O and CH_2N, 294H), 1.09 (s, *t*Bu, 9H).

The signal at 1.09 ppm is attributed to *tert*-butylated amine repeating units. Successful deprotection was shown by the disappearance of the signal at 1.40 ppm (CH_3 Boc).

(MALDI-TOF MS) (*m*/*z*) (*trans*-2-[3-(4-*tert*-butylphenyl)-2-methyl-2-propenylidene]-malononitrile):

(1) Repeating unit: calcd for $C_4H_9N_3O$: 115.0746. Found 115.0714−115.0835.

(2) Main series: calcd for[a] $C_{27}H_{61}N_{14}O_6$: 677.4899; $C_{31}H_{70}N_{17}O_7$: 792.5645; $C_{35}H_{79}N_{20}O_8$: 907.6391; $C_{39}H_{88}N_{23}O_9$: 1022.7137; $C_{43}H_{97}N_{26}O_{10}$: 1137.7883; $C_{47}H_{106}N_{29}O_{11}$: 1252.8629; $C_{51}H_{115}N_{32}O_{12}$: 1367.9375; $C_{55}H_{124}N_{35}O_{13}$: 1483.0121; $C_{59}H_{133}N_{39}O_{14}$: 1598.0867. Found 677.4373 $[M]^+$, n = 4; 792.5162 $[M]^+$, n = 5; 907.5981 $[M]^+$, n = 6; 1022.6764 $[M]^+$, n = 7; 1137.7567 $[M]^+$, n = 8; 1252.8342 $[M]^+$, n = 9; 1367.9177 $[M]^+$, n = 10; 1482.9913 $[M]^+$, n = 11; 1598.0627 $[M]^+$, n = 12 (Figure 7).

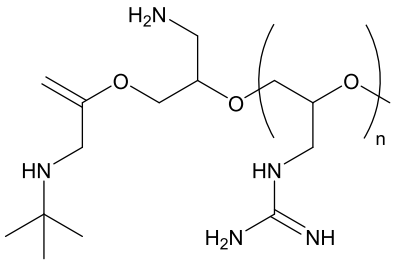

Figure 7. Proposed structure of the products formed under MALDI conditions for the main series of the molecular weight distribution in MS analysis.

(3) Fragmentation peak series (shifted 16 mass units from the main series of the molecular weight distribution):[23] Found 661.3962 $[M-16]^+$, n = 4; 776.4775 $[M-16]^+$, n = 5; 891.5585 $[M-16]^+$, n = 6; 1006.6370 $[M-16]^+$, n = 7; 1121.7172 $[M-16]^+$, n = 8; 1236.7969 $[M-16]^+$, n = 9; 1351.8767 $[M-16]^+$, n = 10; 1466.9503 $[M-16]^+$, n = 11; 1582.0428 $[M-16]^+$, n = 12; 1697.1379 $[M-16]^+$, n = 13.

Nanoparticle Formation and Physicochemical Data. For octa-arginine and PEGtide−siRNA nanoparticle formation, a weighed amount of polymer was diluted in PBS to the required concentration of 1 mg/mL. Amine (N)-to-siRNA phosphate (P) N/P ratios were calculated as previously described[54] for octa-arginine nanoparticles with equivalent masses of cationic polymer used to make PEGtide−siRNA nanoparticles. Various volumes of the cationic polymer solutions were then added to the appropriate amount of 20 μM siRNA to give specific N/P ratios and were diluted in PBS to a final concentration of 1 μM. The polymer−siRNA solutions were then mixed gently with a pipette to ensure homogeneity and were incubated at room temperature for 20−30 min to allow nanoparticle formation.

The size distribution (mean diameter and polydispersity index) and ζ potential of the siRNA nanoparticle dispersions were measured by dynamic light scattering and laser Doppler electrophoresis, respectively, using a Nano-ZS system (Nano series; Malvern Instruments). This measured the mass distribution of the particle size and the electrophoretic mobility of the dispersed particles. Measurements were made at 25 °C with a fixed angle of 137°. The sizes quoted are the *z*-average means (dz) for the nanoparticle hydrodynamic diameter (nm). Calculation of the ζ potential (mV) was performed using the same instrument (from electrophoretic mobility). Following complexation in PBS, the samples were diluted 1 in 50 with deionized water prior to both procedures. This resulted in a final ionic concentration of 2.74 mM NaCl, 0.054 mM KCl, 0.2 mM Na_2HPO_4, and 0.04 mM KH_2PO_4. Both the size and ζ potential were measured five times with an average of 15−20 subscans taken in each measurement.

Multiparameter Cytotoxicity Study of Peptidomimetic siRNA Nanoparticles in Calu-3 Cells. Twenty-four hours prior to transfection, the cells were seeded at 3 × 10^4/well in a 96-well plate and were treated with 100 nM siRNA for 24 h. The selected wells were treated with 120 μM valinomycin or 40 μM carbobenzoxy-L-leucyl-L-leucyl-L-leucinal (MG132) for 24 h as a positive control prior to analysis. Following incubation, the cells were stained and fixed using the Cellomics Multiparameter Cytotoxicity 3 kit (Thermo Scientific, Dublin, Ireland) according to the manufacturer's protocol. Briefly, the cells were live-stained for mitochondrial membrane potential and plasma membrane permeability. The cells were then fixed using 4% paraformaldehyde before staining with Hoechst nuclear stain and fluorescent antibody labeling for cytochrome *c*. Image acquisition was determined using the InCell 1000 High Content Analyzer (GE Healthcare, Buckinghamshire, U.K.). Four random fields were viewed per well, and the various N/P ratios were repeated in quadruplicate. The fluorescence intensity of the dyes was monitored at the excitation and emission wavelengths specific to each dye (i.e., 360 and 460 nm for Hoechst, 480 and 535 nm for the permeability dye, 535 and 600 nm for the mitochondrial membrane potential dye, and 646/674 nm for DyLight 649 conjugates).

The exposure times and hardware autofocus (HWAF) values were varied between experiments to optimize the image quality. Following acquisition of the images, the data were analyzed using InCell 1000 Workstation software and multitarget analysis with a variety of settings for each of the parameters (Table S2). All samples were run in quadruplicate, and the experiment was repeated on three independent occasions. The commercial transfection reagents for in vitro-only use were not assessed for cytotoxicity. However, the various cytotoxic profiles for these vectors were previously reported in several studies.[55−57]

siRNA Nanoparticle Uptake in Calu-3 Cells. Calu-3 cells were seeded at 3 × 10^4 cells/well in a 96-well plate (Nunc) 24 h before experiments. Nanoparticles were formed using electrostatic complexation in a final volume of 125 μL/well in serum-free Dulbecco's modified Eagle's medium (DMEM) using 100 nM fluorescently tagged FITC−siRNA. Nanoparticles, or free

DOI: 10.1021/acsomega.9b00265
ACS Omega 2019, 4, 10078−10088

siRNA controls, were then incubated with the cells at 37 °C and 5% CO_2 for 2, 4 and 24 h. The cells were washed with PBS and fixed using 4% paraformaldehyde. The cells were then stained for f-actin using phalloidin−TRITC and Hoechst nuclear stain. Image analysis was achieved using the InCell 1000 High Content Analyzer. Four random fields were viewed per well, and the various treatments were repeated in quadruplicate. The fluorescence intensity of the dyes was monitored at the excitation and emission wavelengths specific to each dye—i.e., 360 and 460 nm for Hoechst, 480 and 535 nm for FITC−siRNA, and 535 and 600 nm for phalloidin−TRITC. The exposure times and hardware autofocus (HWAF) values were varied to optimize the image quality. After acquisition of the images, the data were analyzed using InCell 1000 Workstation software and multitarget analysis with various settings for each of the parameters (Table S1). Specifically, minimum PEGtide−siRNA nanocomplex diameters were measured using the "organelle" function Workstation software and gated to include only FITC-positive particles of a designated size that were inside cells. These were proofed against negative controls to eliminate background/artifact detection and total particles within cells were counted and averaged. All samples were run in quadruplicate, and the experiment was repeated on three independent occasions.

siRNA Nanoparticle-Mediated Luciferase Knockdown in Calu-3 Cells. Calu-3 cells were seeded at a density of 5×10^4 in 48-well plates 24 h prior to transfection. Thereafter, the cells were first transfected with the luciferase control vector plasmid (Promega, U.K.) and SuperFect transfection reagent (Qiagen, Manchester, U.K.) at a dose of 0.75 μg of pDNA/3 μL of SuperFect in 100 μL of serum-free DMEM per well for 4 h. The cells were then washed three times with warm PBS and transfected with antiluciferase PEGtide−siRNA nanoparticles consisting of either antiluciferase siRNA or negative control siRNA at 100 nM/well in 250 μL of serum-containing media, followed by incubation for 24 h at 37 °C and 5% CO_2.

Control transfections involving siRNA were carried out using the cationic, lipid-based RNAiFect transfection vector (Qiagen, Manchester, U.K.). siRNA (1 μg) was diluted to 100 μL in the supplied Buffer EC-R and vortexed. The appropriate amount of RNAiFect reagent was then added, and the solution was vortexed again for 10 s. The samples were incubated at room temperature for 20 min to allow complex formation. Thereafter, the particles were diluted with serum-containing medium to a final siRNA concentration of 100 nM before adding 250 μL of the diluted solution to the cells.

Luciferase expression was assessed using the luciferase assay system (Promega) and was read using a Wallac 1420 Multilabel Counter (PerkinElmer). The protein expression in each sample was examined using the Micro bicinchoninic acid (BCA) protein assay kit (Pierce) according to the product instructions. All samples were run in quadruplicate, and the experiment was repeated on three independent occasions.

siRNA Nanoparticle-Mediated Luciferase Knockdown in mHypo N41 Cells. The mouse embryonic hypothalamic cell line *mHypoE N*41 was obtained from tebu-bio (Le Perray-en-Yvelines, France) and was maintained in Dulbecco's modified Eagle's medium (DMEM) supplemented with 10% fetal bovine serum in a humidified 37 °C incubator with 5% CO_2. The cells were seeded in 24-well plates at a density of 3.5×10^4 cells/well.

Silencing of an exogenous gene was assessed by measuring the knockdown of the firefly luciferase gene. Cells were seeded in 24-well plates for 1 day before transfection with the luciferase reporter plasmid pGL3 luciferase (1 μg/well) complexed to Lipofectamine 2000 (Invitrogen, Dublin, Ireland) (2.5 μL/μg pDNA) for 4 h. Thereafter, the cells were washed twice with PBS prior to siRNA transfection. siRNA was complexed with PEGtide at varying N/P ratios (N/P = 6, 9, 12, 15, and 30) and was incubated for 20−30 min, followed by dilution in serum-free media without antibiotics. A final volume of media on cells was 0.5 mL containing 100 nM siRNA per well. Nonsilencing siRNA complexed to PEGtide at N/P = 30 was used as a nontargeted control. After 24 h, the cells were lysed with 1× lysis buffer (Promega, Southampton, U.K.). Next, the lysates (20 μL) were assayed for the expression of luciferase by adding 100 μL of luciferin (Promega) and measuring the luminescence in a Junior LB 9059 luminometer (Promega). The total protein levels in each sample were determined using the BCA protein assay (Thermo Scientific, Dublin, Ireland) to allow normalization of luciferase activity. The results were expressed as the percent of gene expression relative to control samples. The data are presented as mean ± SEM.

Control transfections involving siRNA were carried out using the cationic lipid-based transfection reagent Lipofectamine 2000 (Lf2000). Lf2000·siRNA complexes were prepared according to the manufacturer's protocol. Briefly, the required volume of Lf2000 was diluted in 50 μL of OptiMEM, mixed gently, and incubated at RT for 5 min. siRNA was diluted in 50 μL of OptiMEM and was combined with the diluted Lf2000, followed by gentle mixing and incubation at RT for 20 min. One microliter of Lf2000 was used per 20 pmol of siRNA.

Statistical Analysis. The results are expressed as the mean ± standard error of the mean (SEM) using GraphPad Prism 5 software. Two- and one-way analyses of variance (ANOVA) were performed for differences between treatments with p-values <0.05 considered significant, <0.01 very significant, and <0.001 highly significant.

■ ASSOCIATED CONTENT

Supporting Information

The Supporting Information is available free of charge on the ACS Publications website at DOI: 10.1021/acsomega.9b00265.

Analytical data for octa-D-arginine and poly-(glycidylguanidine) and its synthetic intermediates; optimization of pDNA and RNAiFect transfection conditions; and settings for InCell 1000 Workstation analysis (PDF)

■ AUTHOR INFORMATION

Corresponding Author

*E-mail: mdevocelle@rcsi.ie. Phone: 00353 1 402 2176.

ORCID

Sally-Ann Cryan: 0000-0002-3941-496X

Marc Devocelle: 0000-0001-7641-1306

Author Contributions

◆A.H. and A.M.O. contributed equally to this work.

Notes

The authors declare no competing financial interest.

■ ACKNOWLEDGMENTS

This publication was emanated from research conducted with the financial support of the Science Foundation Ireland (SFI) under Grants SFI 07/SRC/B1154 (Irish Drug Delivery Network) to M.D., S.-A.C., A.M.O., A.H., J.M., and C.M.O.;

DOI: 10.1021/acsomega.9b00265
ACS Omega 2019, 4, 10078−10088

Equipment Grant SFI 06/RFP/CHO024/EC07 to M.D. and SFI IvP 13/IA/1840 to S.-A.C. The authors acknowledge the Higher Education Authority, Ireland, under the BioAT program, in Cycle 5 of the Programme for Research in Third-Level Institutions for financial support to E.B.F. They thank Dr. Peter O'Brien and Prof. David Brayden (UCD) for the use of the HCA facility.

■ ADDITIONAL NOTE

[a]The main series of the molecular weight distribution can be assigned to the structure shown in Figure 7, where the secondary amine results from *t*-butylation during polymerization and the primary amine results from incomplete guanylation during the penultimate step. The vinyloxy and methoxy ends are modifications formed by pyrolysis during MALDI analysis.[22]

■ REFERENCES

(1) Garber, K. Worth the RISC? *Nat. Biotechnol.* **2017**, *35*, 198.
(2) Wittrup, A.; Lieberman, J. Knocking down disease: a progress report on siRNA therapeutics. *Nat. Rev. Genet.* **2015**, *16*, 543.
(3) Tagalakis, A. D.; Munye, M. M.; Ivanova, R.; Chen, H.; Smith, C. M.; Aldossary, A. M.; Rosa, L. Z.; Moulding, D.; Barnes, J. L.; Kafetzis, K. N.; Jones, S. A.; Baines, D. L.; Moss, G. W. J.; O'Callaghan, C.; McAnulty, R. J.; Hart, S. L. Effective silencing of ENaC by siRNA delivered with epithelial-targeted nanocomplexes in human cystic fibrosis cells and in mouse lung. *Thorax* **2018**, *73*, 847−856.
(4) Manunta, M. D. I.; Tagalakis, A. D.; Attwood, M.; Aldossary, A. M.; Barnes, J. L.; Munye, M. M.; Weng, A.; McAnulty, R. J.; Hart, S. L. Delivery of ENaC siRNA to epithelial cells mediated by a targeted nanocomplex: a therapeutic strategy for cystic fibrosis. *Sci. Rep.* **2017**, *7*, No. 700.
(5) Suhr, O. B.; Coelho, T.; Buades, J.; Pouget, J.; Conceicao, I.; Berk, J.; Schmidt, H.; Waddington-Cruz, M.; Campistol, J. M.; Bettencourt, B. R.; Vaishnaw, A.; Gollob, J.; Adams, D. Efficacy and safety of patisiran for familial amyloidotic polyneuropathy: a phase II multi-dose study. *Orphanet J. Rare Dis.* **2015**, *10*, No. 109.
(6) Suhorutsenko, J.; Oskolkov, N.; Arukuusk, P.; Kurrikoff, K.; Eriste, E.; Copolovici, D. M.; Langel, U. Cell-penetrating peptides, PepFects, show no evidence of toxicity and immunogenicity in vitro and in vivo. *Bioconjugate Chem.* **2011**, *22*, 2255−2262.
(7) Mitchell, D. J.; Kim, D. T.; Steinman, L.; Fathman, C. G.; Rothbard, J. B. Polyarginine enters cells more efficiently than other polycationic homopolymers. *J. Pept. Res.* **2000**, *56*, 318−325.
(8) Henninot, A.; Collins, J. C.; Nuss, J. M. The Current State of Peptide Drug Discovery: Back to the Future? *J. Med. Chem.* **2018**, *61*, 1382−1414.
(9) Ripka, A. S.; Rich, D. H. Peptidomimetic design. *Curr. Opin. Chem. Biol.* **1998**, *2*, 441−452.
(10) Qvit, N.; Rubin, S. J. S.; Urban, T. J.; Mochly-Rosen, D.; Gross, E. R. Peptidomimetic therapeutics: scientific approaches and opportunities. *Drug Discovery Today* **2017**, *22*, 454−462.
(11) Avan, I.; Hall, C. D.; Katritzky, A. R. Peptidomimetics via modifications of amino acids and peptide bonds. *Chem. Soc. Rev.* **2014**, *43*, 3575−3594.
(12) Giuliani, A.; Pirri, G.; Bozzi, A.; Di Giulio, A.; Aschi, M.; Rinaldi, A. Antimicrobial peptides: natural templates for synthetic membrane-active compounds. *Cell. Mol. Life Sci.* **2008**, *65*, 2450−2460.
(13) Giuliani, A.; Rinaldi, A. Beyond natural antimicrobial peptides: multimeric peptides and other peptidomimetic approaches. *Cell. Mol. Life Sci.* **2011**, *68*, 2255−2266.
(14) Peng, L.; Liu, R.; Marik, J.; Wang, X.; Takada, Y.; Lam, K. S. Combinatorial chemistry identifies high-affinity peptidomimetics against $\alpha 4\beta 1$ integrin for in vivo tumor imaging. *Nat. Chem. Biol.* **2006**, *2*, 381−389.
(15) Rerat, V.; Dive, G.; Cordi, A. A.; Tucker, G. C.; Bareille, R.; Amédée, J.; Bordenave, L.; Marchand-Brynaert, J. $\alpha v\beta 3$ Integrin-Targeting Arg-Gly-Asp (RGD) Peptidomimetics Containing Oligo-ethylene Glycol (OEG) Spacers. *J. Med. Chem.* **2009**, *52*, 7029−7043.
(16) Merkel, O. M.; Germershaus, O.; Wada, C. K.; Tarcha, P. J.; Merdan, T.; Kissel, T. Integrin $\alpha v\beta 3$ Targeted Gene Delivery Using RGD Peptidomimetic Conjugates with Copolymers of PEGylated Poly(ethylene imine). *Bioconjugate Chem.* **2009**, *20*, 1270−1280.
(17) Jing, X.; Kasimova, M. R.; Simonsen, A. H.; Jorgensen, L.; Malmsten, M.; Franzyk, H.; Foged, C.; Nielsen, H. M. Interaction of Peptidomimetics with Bilayer Membranes: Biophysical Characterization and Cellular Uptake. *Langmuir* **2012**, *28*, 5167−5175.
(18) Harris, J. M.; Chess, R. B. Effect of pegylation on pharmaceuticals. *Nat. Rev. Drug Discovery* **2003**, *2*, 214−221.
(19) Herzberger, J.; Niederer, K.; Pohlit, H.; Seiwert, J.; Worm, M.; Wurm, F. R.; Frey, H. Polymerization of Ethylene Oxide, Propylene Oxide, and Other Alkylene Oxides: Synthesis, Novel Polymer Architectures, and Bioconjugation. *Chem. Rev.* **2016**, *116*, 2170−2243.
(20) Gao, J.; Chen, P.; Singh, Y.; Zhang, X.; Szekely, Z.; Stein, S.; Sinko, P. J. Novel Monodisperse PEGtide Dendrons: Design, Fabrication, and Evaluation of Mannose Receptor-Mediated Macrophage Targeting. *Bioconjugate Chem.* **2013**, *24*, 1332−1344.
(21) Krakowiak, K. E.; Bradshaw, J. S. Thermal Removal of Boc-Protecting Groups During Preparation of Open-Chain Polyamines. *Synth. Commun.* **1996**, *26*, 3999−4004.
(22) Marie, A.; Fournier, F.; Tabet, J. C. Characterization of Synthetic Polymers by MALDI-TOF/MS: Investigation into New Methods of Sample Target Preparation and Consequence on Mass Spectrum Finger Print. *Anal. Chem.* **2000**, *72*, 5106−5114.
(23) Wetzel, S. J.; Guttman, C. M.; Flynn, K. M.; Filliben, J. J. Significant Parameters in the Optimization of MALDI-TOF-MS for Synthetic Polymers†. *J. Am. Soc. Mass Spectrom.* **2006**, *17*, 246−252.
(24) Hruby, V. J. Houben−Weyl Methods of Organic Chemistry. Volume E22A. Synthesis of Peptides and Peptidomimetics Edited by Murray Goodman, Arthur Felix, Luis Moroder, and Claudio Toniolo. Georg Thieme Verlag, Stuttgart, Germany. 2001. xxvii + 901 pp. 18 × 26 cm. ISBN 3 132 19604 5. 1840 euro. *J. Med. Chem.* **2002**, *45*, 5187.
(25) deRonde, B. M.; Tew, G. N. Development of protein mimics for intracellular delivery. *Biopolymers* **2015**, *104*, 265−280.
(26) Funhoff, A. M.; van Nostrum, C. F.; Lok, M. C.; Fretz, M. M.; Crommelin, D. J. A.; Hennink, W. E. Poly(3-guanidinopropyl methacrylate): A Novel Cationic Polymer for Gene Delivery. *Bioconjugate Chem.* **2004**, *15*, 1212−1220.
(27) Caffrey, L. M.; deRonde, B. M.; Minter, L. M.; Tew, G. N. Mapping Optimal Charge Density and Length of ROMP-Based PTDMs for siRNA Internalization. *Biomacromolecules* **2016**, *17*, 3205−3212.
(28) Verdurmen, W.P. R.; Bovee-Geurts, P. H.; Wadhwani, P.; Ulrich, A. S.; Hällbrink, M.; van Kuppevelt, T. H.; Brock, R.; Brock, H. Preferential Uptake of L- versus D-Amino Acid Cell-Penetrating Peptides in a Cell Type-Dependent Manner. *Chem. Biol.* **2011**, *18*, 1000−1010.
(29) Raftery, R.; Brien, F.; Cryan, S.-A. Chitosan for Gene Delivery and Orthopedic Tissue Engineering Applications. *Molecules* **2013**, *18*, 5611.
(30) Wang, X.; Niu, D.; Hu, C.; Li, P. Polyethyleneimine-Based Nanocarriers for Gene Delivery. *Curr. Pharm. Des.* **2015**, *21*, 6140−6156.
(31) Zheng, M.; Librizzi, D.; Kılıç, A.; Liu, Y.; Renz, H.; Merkel, O. M.; Kissel, T. Enhancing in vivo circulation and siRNA delivery with biodegradable polyethylenimine-graft-polycaprolactone-block-poly(ethylene glycol) copolymers. *Biomaterials* **2012**, *33*, 6551−6558.
(32) Wu, Y.; Wang, W.; Chen, Y.; Huang, K.; Shuai, X.; Chen, Q.; Li, X.; Lian, G. The investigation of polymer-siRNA nanoparticle for gene therapy of gastric cancer in vitro. *Int. J. Nanomed.* **2010**, *5*, 129−136.
(33) Ezzat, K.; El Andaloussi, S.; Zaghloul, E. M.; Lehto, T.; Lindberg, S.; Moreno, P. M. D.; Viola, J. R.; Magdy, T.; Abdo, R.; Guterstam, P.; Sillard, R.; Hammond, S. M.; Wood, M. J. A.; Arzumanov, A. A.; Gait, M. J.; Smith, C. I. E.; Hällbrink, M.; Langel, Ü. PepFect 14, a novel cell-penetrating peptide for oligonucleotide delivery in solution and as solid formulation. *Nucleic Acids Res.* **2011**, *39*, 5284−5298.

DOI: 10.1021/acsomega.9b00265
ACS Omega 2019, 4, 10078−10088

(34) Regberg, J.; Vasconcelos, L.; Madani, F.; Langel, Ü.; Hällbrink, M. pH-responsive PepFect cell-penetrating peptides. *Int. J. Pharm.* **2016**, *501*, 32−38.
(35) Zeng, X.; de Groot, A. M.; Sijts, A. J. A. M.; Broere, F.; Oude Blenke, E.; Colombo, S.; van Eden, W.; Franzyk, H.; Nielsen, H. M.; Foged, C. Surface coating of siRNA−peptidomimetic nano-self-assemblies with anionic lipid bilayers: enhanced gene silencing and reduced adverse effects in vitro. *Nanoscale* **2015**, *7*, 19687−19698.
(36) Hibbitts, A.; O'Mahony, A. M.; Forde, E.; Nolan, L.; Ogier, J.; Desgranges, S.; Darcy, R.; Macloughlin, R.; O'Driscoll, C. M.; Cryan, S. A. Early-Stage Development of Novel Cyclodextrin-siRNA Nanocomplexes Allows for Successful Postnebulization Transfection of Bronchial Epithelial Cells. *J. Aerosol Med. Pulm. Drug Delivery* **2014**, 466−477.
(37) Sardo, C.; Craparo, E. F.; Porsio, B.; Giammona, G.; Cavallaro, G. Improvements in Rational Design Strategies of Inulin Derivative Polycation for siRNA Delivery. *Biomacromolecules* **2016**, *17*, 2352−2366.
(38) Mao, H. Q.; Roy, K.; Troung-Le, V. L.; Janes, K. A.; Lin, K. Y.; Wang, Y.; August, J. T.; Leong, K. W. Chitosan-DNA nanoparticles as gene carriers: synthesis, characterization and transfection efficiency. *J. Controlled Release* **2001**, *70*, 399−421.
(39) Moore, N. M.; Barbour, T. R.; Sakiyama-Elbert, S. E. Synthesis and Characterization of Four-Arm Poly(ethylene glycol)-Based Gene Delivery Vehicles Coupled to Integrin and DNA-Binding Peptides. *Mol. Pharmaceutics* **2008**, *5*, 140−150.
(40) Veiman, K.-L.; Künnapuu, K.; Lehto, T.; Kiisholts, K.; Pärn, K.; Langel, Ü.; Kurrikoff, K. PEG shielded MMP sensitive CPPs for efficient and tumor specific gene delivery in vivo. *J. Controlled Release* **2015**, *209*, 238−247.
(41) Kummitha, C. M.; Malamas, A. S.; Lu, Z. R. Albumin pre-coating enhances intracellular siRNA delivery of multifunctional amphiphile/siRNA nanoparticles. *Int. J. Nanomed.* **2012**, *7*, 5205−5214.
(42) Strojan, K.; Leonardi, A.; Bregar, V. B.; Krizaj, I.; Svete, J.; Pavlin, M. Dispersion of Nanoparticles in Different Media Importantly Determines the Composition of Their Protein Corona. *PLoS One* **2017**, *12*, No. e0169552.
(43) Yamamoto, T.; Yamada, A.; Yoshimura, Y.; Terada, H.; Shinohara, Y. The mechanisms of the release of cytochrome C from mitochondria revealed by proteomics analysis. *Yakugaku Zasshi* **2012**, *132*, 1099−1104.
(44) Bröker, L. E.; Kruyt, F. A. E.; Giaccone, G. Cell Death Independent of Caspases: A Review. *Clin. Cancer Res.* **2005**, *11*, 3155−3162.
(45) Breunig, M.; Lungwitz, U.; Liebl, R.; Goepferich, A. Breaking up the correlation between efficacy and toxicity for nonviral gene delivery. *Proc. Natl. Acad. Sci. U.S.A.* **2007**, *104*, 14454−14459.
(46) O'Mahony, A. M.; Desgranges, S.; Ogier, J.; Quinlan, A.; Devocelle, M.; Darcy, R.; Cryan, J. F.; O'Driscoll, C. M. In vitro investigations of the efficacy of cyclodextrin-siRNA complexes modified with lipid-PEG-Octaarginine: towards a formulation strategy for non-viral neuronal siRNA delivery. *Pharm. Res.* **2013**, *30*, 1086−1098.
(47) Fröhlich, E. The role of surface charge in cellular uptake and cytotoxicity of medical nanoparticles. *Int. J. Nanomed.* **2012**, *7*, 5577−5591.
(48) Yang, R.; Yang, S.-G.; Shim, W.-S.; Cui, F.; Cheng, G.; Kim, I.-W.; Kim, D.-D.; Chung, S.-J.; Shim, C.-K. Lung-Specific Delivery of Paclitaxel by Chitosan-Modified PLGA Nanoparticles Via Transient Formation of Microaggregates. *J. Pharm. Sci.* **2009**, *98*, 970−984.
(49) Minami, K.; Okamoto, K.; Doi, K.; Harano, K.; Noiri, E.; Nakamura, E. siRNA delivery targeting to the lung via agglutination-induced accumulation and clearance of cationic tetraamino fullerene. *Sci. Rep.* **2015**, *4*, No. 4916.
(50) Sahay, G.; Querbes, W.; Alabi, C.; Eltoukhy, A.; Sarkar, S.; Zurenko, C.; Karagiannis, E.; Love, K.; Chen, D.; Zoncu, R.; Buganim, Y.; Schroeder, A.; Langer, R.; Anderson, D. G. Efficiency of siRNA delivery by lipid nanoparticles is limited by endocytic recycling. *Nat. Biotechnol.* **2013**, *31*, 653−658.
(51) Gilleron, J.; Querbes, W.; Zeigerer, A.; Borodovsky, A.; Marsico, G.; Schubert, U.; Manygoats, K.; Seifert, S.; Andree, C.; Stoter, M.; Epstein-Barash, H.; Zhang, L.; Koteliansky, V.; Fitzgerald, K.; Fava, E.; Bickle, M.; Kalaidzidis, Y.; Akinc, A.; Maier, M.; Zerial, M. Image-based analysis of lipid nanoparticle-mediated siRNA delivery, intracellular trafficking and endosomal escape. *Nat. Biotechnol.* **2013**, *31*, 638−646.
(52) Merrifield, B. Solid phase synthesis. *Science* **1986**, *232*, 341−347.
(53) Carpino, L. A.; Han, G. Y. 9-Fluorenylmethoxycarbonyl amino-protecting group. *J. Org. Chem.* **1972**, *37*, 3404−3409.
(54) Zhao, Q.-Q.; Chen, J.-L.; Lv, T.-F.; He, C.-X.; Tang, G.-P.; Liang, W.-Q.; Tabata, Y.; Gao, J.-Q. N/P Ratio Significantly Influences the Transfection Efficiency and Cytotoxicity of a Polyethylenimine/Chitosan/DNA Complex. *Biol. Pharm. Bull.* **2009**, *32*, 706−710.
(55) Breunig, M.; Lungwitz, U.; Liebl, R.; Goepferich, A. Breaking up the correlation between efficacy and toxicity for nonviral gene delivery. *Proc. Natl. Acad. Sci. U.S.A.* **2007**, *104*, 14454−14459.
(56) Axel, D. I.; Spyridopoulos, I.; Riessen, R.; Runge, H.; Viebahn, R.; Karsch, K. R. Toxicity, uptake kinetics and efficacy of new transfection reagents: increase of oligonucleotide uptake. *J. Vasc. Res.* **2000**, *37*, 221−234.
(57) Arbab, A. S.; Yocum, G. T.; Wilson, L. B.; Parwana, A.; Jordan, E. K.; Kalish, H.; Frank, J. A. Comparison of transfection agents in forming complexes with ferumoxides, cell labeling efficiency, and cellular viability. *Mol. Imaging* **2004**, *3*, 24−32.

DOI: 10.1021/acsomega.9b00265
ACS Omega 2019, 4, 10078−10088